Geophysical Research Letters

RESEARCH LETTER
10.1029/2024GL112059

Optimal Atmospheric Heat Sources for the Interannual Variability of South Asian Summer Monsoon

Tong Lu[1,2], **Kaiming Hu**[1,3], **Gang Huang**[1,2,4], **and Ya Wang**[1]

[1]Key Laboratory of Earth System Numerical Modeling and Application, Institute of Atmospheric Physics, Chinese Academy of Sciences, Beijing, China, [2]College of Earth and Planetary Sciences, University of Chinese Academy of Sciences, Beijing, China, [3]Center for Monsoon System Research, Institute of Atmospheric Physics, Chinese Academy of Sciences, Beijing, China, [4]Laboratory for Regional Oceanography and Numerical Modeling, Qingdao National Laboratory for Marine Science and Technology, Qingdao, China

Abstract Using a Green's function-like approach, this study identifies optimal atmospheric heat sources for the two leading modes of South Asian Summer Monsoon (SASM) interannual variability. Optimal heating for the first mode, characterized by a lower-level anomalous anticyclone over northern Bay of Bengal (BOB), is distributed over the Arabian Sea and tropical eastern Indian Ocean (EIO)-Maritime Continent, with cooling over the BOB-western North Pacific. In contrast, heating over the tropical southwestern Indian Ocean and equatorial Atlantic, along with cooling over the tropical EIO-western Pacific, optimally drives the second mode, featuring an anomalous anticyclone over central-northern India. El Niño/Southern Oscillation indirectly influences SASM by triggering heat sources resembling these optimal patterns. Other sea surface temperatures (SSTs), like those over equatorial Atlantic, can also generate similar heating structures, causing corresponding SASM anomalies. This suggests that the impact of SST modes on SASM depends on the similarity of induced heat sources to optimal patterns.

Plain Language Summary The principal origins of South Asian summer monsoon (SASM) interannual variability are rooted in the combined modulation of three tropical oceans, which challenges its prediction due to complex multi-ocean interactions. Atmospheric heat sources, however, can directly impact SASM, acting as a bridge connecting sea surface temperature (SST) and SASM. Here we identify optimal atmospheric heat sources for the two leading modes of SASM interannual variability using a Green's function-like approach. Optimal heating for the first mode, characterized by a lower-level anomalous anticyclone over northern Bay of Bengal (BOB), is distributed over the Arabian Sea and the tropical eastern Indian Ocean (EIO)-Maritime Continent, with cooling over the BOB-western North Pacific. In contrast, heating over the tropical southwestern Indian Ocean and equatorial Atlantic, along with cooling over the tropical EIO-western Pacific, optimally drives the second SASM mode, featuring a lower-level anomalous anticyclone over central-northern India. El Niño/Southern Oscillation indirectly influences SASM by triggering heat sources resembling these optimal patterns. Other SSTs, such as those over the equatorial Atlantic, can also generate similar heating structures as the optimal heat sources, further impacting corresponding SASM modes. Optimal heat sources provide a possible way to understand the combined effects of different SST modes on SASM.

Key Points:

- Optimal heat sources for the South Asian summer monsoon (SASM) interannual variability are identified using a Green's function-like method
- The El Niño/Southern Oscillation indirectly impacts SASM by triggering heat sources resembling the optimal patterns
- Other sea surface temperature anomalies can also generate similar heating structures to the optimal patterns, leading to SASM anomalies

Supporting Information:

Supporting Information may be found in the online version of this article.

Correspondence to:

K. Hu and G. Huang,
hkm@mail.iap.ac.cn;
hg@mail.iap.ac.cn

Citation:

Lu, T., Hu, K., Huang, G., & Wang, Y. (2024). Optimal atmospheric heat sources for the interannual variability of South Asian summer monsoon. *Geophysical Research Letters*, *51*, e2024GL112059. https://doi.org/10.1029/2024GL112059

Received 17 AUG 2024
Accepted 27 OCT 2024

Author Contributions:

Conceptualization: Tong Lu, Kaiming Hu, Gang Huang
Data curation: Tong Lu, Kaiming Hu
Formal analysis: Tong Lu, Kaiming Hu, Gang Huang, Ya Wang
Funding acquisition: Kaiming Hu, Gang Huang
Investigation: Tong Lu
Methodology: Tong Lu, Kaiming Hu, Ya Wang
Software: Tong Lu
Supervision: Kaiming Hu, Gang Huang, Ya Wang
Validation: Tong Lu
Visualization: Tong Lu

1. Introduction

The South Asian summer monsoon (SASM) exhibits significant interannual variations in atmospheric circulation and rainfall, influencing the most densely populated region in the world (Turner & Annamalai, 2012). The SASM interannual variability frequently triggers climate-related disasters, which not only severely impact local agriculture and water security (H. Tang et al., 2022; Zhou et al., 2019), but also influence remote climate through atmospheric teleconnections (Ding & Wang, 2005; R. Wu, 2017). For instance, the abnormally strong SASM of 2022 resulted in heavy rainfall in Pakistan (Li et al., 2023) and triggered quasi-stationary Rossby waves, leading to sustained heatwaves in the Yangtze River Basin (S. Tang et al., 2023) and marine heatwaves in the western North Pacific (Song et al., 2024).

Considerable efforts have been devoted to understanding the mechanisms and prediction of SASM. The principal origins of SASM interannual variability are rooted in oceanic forcing. It is significantly impacted by the decaying and developing phases of El Niño/Southern Oscillation (ENSO; Mishra et al., 2012; Webster & Yang, 1992; Zhang et al., 2022). A tripolar precipitation pattern tends to occur in South Asia during decaying ENSO summer

Writing – original draft: Tong Lu
Writing – review & editing: Kaiming Hu, Gang Huang, Ya Wang

(Figures 1a and 1b), associated with the Indo-Western Pacific Ocean Capacitor mode (IPOC; Chowdary et al., 2019; Darshana et al., 2022; Xie et al., 2016). During developing El Niño (La Niña) summers, precipitation tends to decrease (increase) over central-northern India (Figures 1c and 1d) through Walker circulation (Lin et al., 2023, 2024). However, the ENSO–SASM relationship is unstable (Chang et al., 2001; Kumar et al., 1999, 2006). One major reason arises from the influence of other sea surface temperature (SST) interannual variability. The intensified Indian Ocean Dipole can weaken the ENSO–SASM relationship (Ashok et al., 2001), whereas summer tropical Indian Ocean SST contributes to restoring the relationship between ENSO and SASM precipitation (Yu et al., 2021). The equatorial Atlantic SST zonal mode (Sabeerali et al., 2019) and North Atlantic SST anomalies (Rajeevan & Sridhar, 2008) can influence SASM precipitation through the Kelvin and Rossby wave response, respectively. Consequently, the combined modulation from the Pacific, Indian, and Atlantic Oceans makes SASM prediction challenging due to the complexity of multi-ocean interactions.

The different SST signals mentioned above mainly influence SASM through atmospheric heat sources (Gill, 1980; Hoskins & Rodwell, 1995). Therefore, identifying the most effective atmospheric heat sources for SASM interannual variability can establish the linkage between SST and SASM. When heat sources induced by a specific SST pattern match the optimal patterns for SASM interannual variability, they can significantly impact SASM. However, the coupling of tropical circulation and atmospheric heat sources complicates their causal relationship in observations (Emanuel et al., 1994). Branstator (1985) proposed the Green's function method, simplifying the responses of a linear system to external forcing as integrals of the Green's function results weighted by the forcing distribution. This method, ensuring the independence of responses to each localized forcing, can effectively identify the optimal forcings of a linear system (Bloch-Johnson et al., 2024; Harrop et al., 2018; Liu et al., 2018, 2022; J. Lu et al., 2020; Y. Wu et al., 2021). A similar method has been employed to investigate the optimal heat sources for the western North Pacific summer monsoon based on the linear baroclinic model (LBM; K. Hu & Long, 2019; Watanabe & Kimoto, 2000). Consequently, this study will utilize this method (hereafter LBM Green's function experiment) to identify the optimal atmospheric heat sources for the two leading modes of SASM interannual variability.

2. Data, Methods, and Model

2.1. Data

The data sets employed in this study include (a) the monthly SST with a 1.0° × 1.0° horizontal resolution from the Hadley Centre Sea Ice and Sea Surface Temperature (HadISST) data set (Rayner et al., 2003); (b) the monthly precipitation with a horizontal resolution of 0.5° × 0.5° from the Climate Research Unit (CRU) TS v.4.07 data set (Harris et al., 2020); (c) the monthly wind at 2.5° × 2.5° horizontal resolution from the fifth-generation ECMWF reanalysis for the global climate and weather (ERA5; Hersbach et al., 2023); (d) the daily wind and temperature from the National Centers for Environmental Prediction-Department of Energy Atmospheric Reanalysis 2 (NCEP2; Kanamitsu et al., 2002) at a resolution of 2.5° × 2.5°. All data sets cover the period of 1979–2022.

2.2. Methods

To focus on the interannual variability, the 9-year running means of all variables were removed. The significance of correlation coefficients and regression coefficients was estimated using the Student's *t*-test. To track ENSO occurrences, the Niño-3.4 index was calculated as the sea surface temperature anomaly (SSTA) averaged over 5°S–5°N, 120°–170°W in December-February (DJF) and June-August (JJA). The Indian monsoon trough index (IMTI; Zhang et al., 2022) was defined as the 850-hPa zonal wind over 10°–18°N, 85°–100°E minus that over 23°–27°N, 83°–95°E. Following B. Wang et al. (2001), the Indian monsoon index (IMI) was defined as the horizontal shear of 850-hPa zonal wind between 5°–15°N, 40°–80°E and 20°–30°N, 70°–90°E.

The atmospheric apparent heat source (Q_1), representing the total diabatic heating and subgrid-scale heat flux convergences, was given by the following formula (Yanai et al., 1973):

$$Q_1 = c_p \frac{\partial T}{\partial t} - c_p(\omega\sigma - V \cdot \nabla T), \quad (1)$$

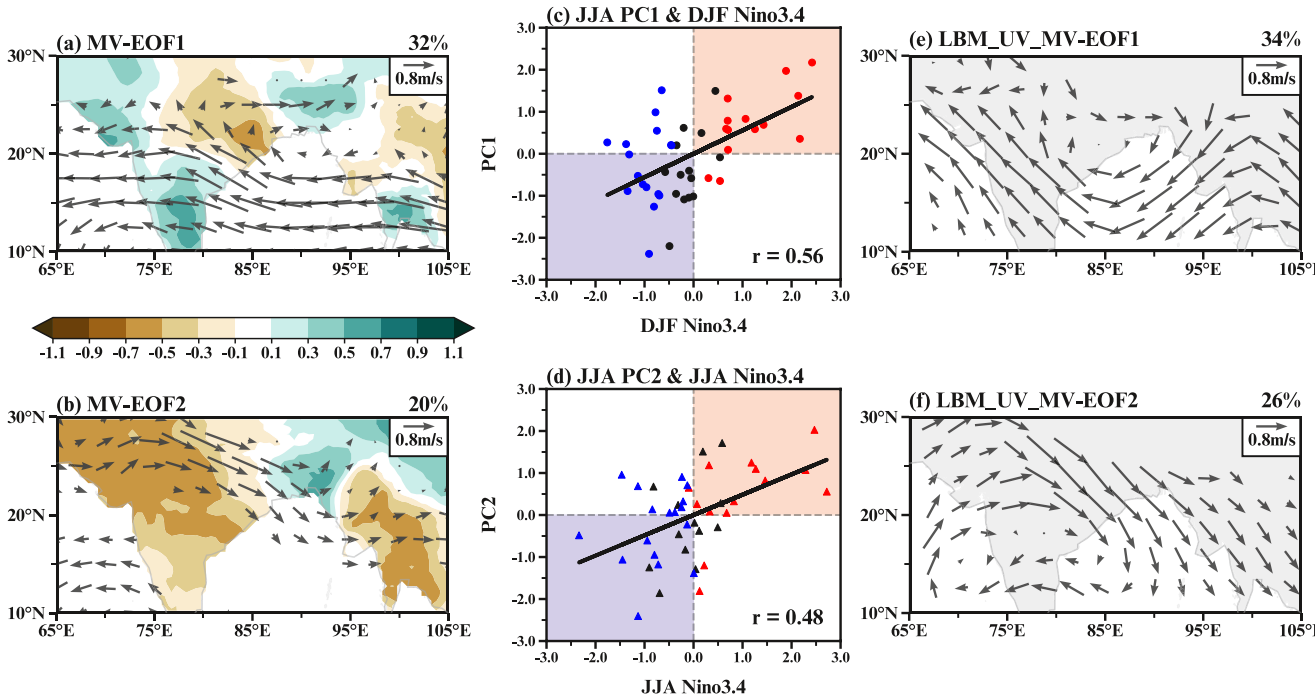

Figure 1. (a and b) Spatial patterns of the two leading MV-EOF modes for the JJA precipitation (shading; mm day^{-1}) and 850-hPa zonal wind. To display the full horizontal wind vector, the 850-hPa winds (vectors; m s^{-1}) are regressed onto the two leading PCs, respectively. Only winds passing the 95% confidence level are shown. (c and d) The scatterplot of PC1 (PC2) and the DJF (JJA) Niño-3.4. Red and blue dots (triangles) denote the El Niño and La Niña decaying (developing) years identified by the Climate Prediction Center. (e and f) Spatial patterns of the two leading MV-EOF modes for the JJA 850-hPa winds among 132 diabatic forcing responses in the LBM Green's function experiment.

where $\sigma = \left(\frac{RT}{c_p p}\right) - \left(\frac{\partial T}{\partial p}\right)$ represents the static stability. c_p and R denote the specific heat at constant pressure (1,004 J K^{-1} kg^{-1}) and the gas constant. T, t, p, ω, and V denote the temperature, time, pressure, vertical velocity, and horizontal velocity vector, respectively. We calculated the vertically averaged Q_1 from the surface through 100-hPa to analyze the atmospheric heat source in observations.

2.3. Model

The LBM (Watanabe & Kimoto, 2000) has been widely employed to investigate atmospheric responses to anomalous diabatic forcing (P. Hu et al., 2024; Y. Wang et al., 2023). The dry version of LBM, suitable for analyzing individual responses to regional heat sources (R. Lu & Lin, 2009), was utilized based on the primitive equations linearized about the observed JJA basic state. The model was run at a horizontal resolution of T42 with 20 sigma levels in the vertical. To obtain steady responses, we integrated the LBM for 50 days and used the averages from 30 to 50 days.

3. Results

3.1. Dominant Modes of SASM Interannual Variability

Considering that precipitation and zonal wind are frequently used to depict the Asian summer monsoon (P. Hu et al., 2022; Xiang & Wang, 2013), the two dominant modes of SASM were identified through multivariate empirical orthogonal function analysis (MV-EOF; B. Wang, 1992) on terrestrial precipitation and 850-hPa zonal wind over South Asia (10°–30°N, 65°–105°E; Zhang et al., 2022) in JJA. The two leading modes account for 32% and 20% of the total variance, respectively, well separated by the criterion of North et al. (1982).

The spatial pattern of the first MV-EOF mode features a lower-level anomalous anticyclone over the northern Bay of Bengal (BOB) and a remarkable tripolar terrestrial precipitation, with negative anomalies in northeastern India and the northcentral Indo-China Peninsula, and positive anomalies on either side (Figure 1a). The first SASM

mode reflects the intensity and zonal position of the Indian monsoon trough and is highly correlated with IMTI, with a correlation coefficient of 0.96 between the first principal components (PC1) and IMTI. The second MV-EOF mode characterizes a lower-level anomalous anticyclone over central-northern India, accompanied by positive terrestrial precipitation anomalies in the northern BOB and negative anomalies elsewhere in South Asia (Figure 1b), which correlates well with IMI ($r = 0.85$ between PC2 and IMI).

Both SASM modes are related to ENSO (Mishra et al., 2012; Zhang et al., 2022). PC1 is closely related to the preceding DJF Niño-3.4 ($r = 0.56$, $p < 0.01$; Figure 1c), accompanied by positive SSTAs in the cold tongue region, peaking in winter and dissipating by summer (Figure S1a in Supporting Information S1). The correlation between PC2 and the concurrent JJA Niño-3.4 is $r = 0.48$ ($p < 0.01$; Figure 1d), associated with positive SSTAs in the cold tongue region during summer (Figure S1b in Supporting Information S1). Note that some ENSO years are quite deviated from the fitting lines, indicating an unstable ENSO–SASM relationship.

3.2. Optimal Atmospheric Heat Sources of SASM Interannual Variability

To evaluate the sensitivity of each regional heat source to SASM interannual variability, we conducted the LBM Green's function experiment (Branstator, 1985; K. Hu & Long, 2019). The region within 55°N and 55°S was divided into 132 uniform subregions, each with a size of 10° latitude × 30° longitude. In each subregion, we prescribed an ideal heat source with a peak of 1 K/day at the 0.45 sigma level using the LBM model. Figure S2 in Supporting Information S1 shows the horizontal and vertical distributions of the atmospheric heat sources.

We first identified the two leading MV-EOF modes for the JJA 850-hPa winds among 132 diabatic forcing responses (Figures 1e and 1f), both passing North's test. The spatial pattern of MV-EOF1 features an anomalous anticyclone over northern BOB, while MV-EOF2 shows an anomalous anticyclone over central-northern India. Since heat sources in all 132 experiments are uniformly distributed between 55°N and 55°S and are independent of one another, the two leading MV-EOF modes in the LBM Green's function experiment are considered to be the preferred modes (Branstator, 1985), which can be easily triggered by external forcings. These patterns from LBM resemble the observed results respectively (Figures 1a and 1b), indicating the first two observed SASM modes are also kinds of preferred modes. Due to the consistency of experiments and observations, further studies are based on the LBM Green's function approach.

Since the IMTI describes the anomalous anticyclone over the northern BOB, a larger IMTI value simulated by LBM indicates a greater impact of the corresponding heat source on the first SASM mode. Therefore, we used the IMTI simulated by each heat source to evaluate the first SASM mode's sensitivity (Figure 2a). In Figure 2a, positive values indicate diabatic heating enhances the first SASM mode, and vice versa. The result suggests that the first mode is sensitive to the heating over the Arabian Sea, tropical eastern Indian Ocean-Maritime Continent (EIO-MC), southern Africa, and southern Mediterranean Sea, and the cooling over the Bay of Bengal-western North Pacific (BOB-WNP), Caspian Sea, and western Europe. Similarly, the IMI can well reflect the anomalous anticyclone over central-northern India and is therefore used to represent the contribution of each heat source to the second SASM mode (Figure 2b), with sensitivity to the heating over the tropical southwestern Indian Ocean (SWIO), equatorial Atlantic, Arabian Sea, and Caspian Sea, and the cooling over the tropical eastern Indian Ocean-western Pacific (EIO-WP) and central and western Europe.

Figures 2c and 2d show the observed Q_1 associated with the PCs. There is significant diabatic heating related to PC1 over the Arabian Sea, tropical EIO-MC, and tropical North Atlantic, with cooling over the BOB-WNP and the western and central equatorial Pacific. PC2 is significantly associated with diabatic heating over the equatorial Pacific, SWIO, and equatorial Atlantic, along with cooling over the tropical EIO-WP. These patterns are similar to those from the LBM Green's function experiment. Note that there are also differences between the experiments and observations. The reasons may arise from three aspects. First, unlike the idealized LBM, observed heat sources are impossible to occur in regions with low climatological rainfall, such as the southern Mediterranean Sea. Second, the dry LBM cannot capture indirect physical processes. For example, in observations, the equatorial diabatic cooling near 170°E can trigger an anomalous anticyclone to its northwest, which could in turn induce off-equatorial rainfall anomalies, further contributing to the PC1-related anticyclone in the Indo-Northwest Pacific (K. Hu & Long, 2019). Another example is that diabatic heating induced by ENSO over the equatorial central and eastern Pacific can lead to diabatic cooling over the tropical EIO-WP via the Walker circulation, indirectly affecting the second SASM mode in observations (B. Wang et al., 2017). These indirect processes described above cannot be reproduced by the dry LBM. Third, due to the coupling of tropical circulation and convection in

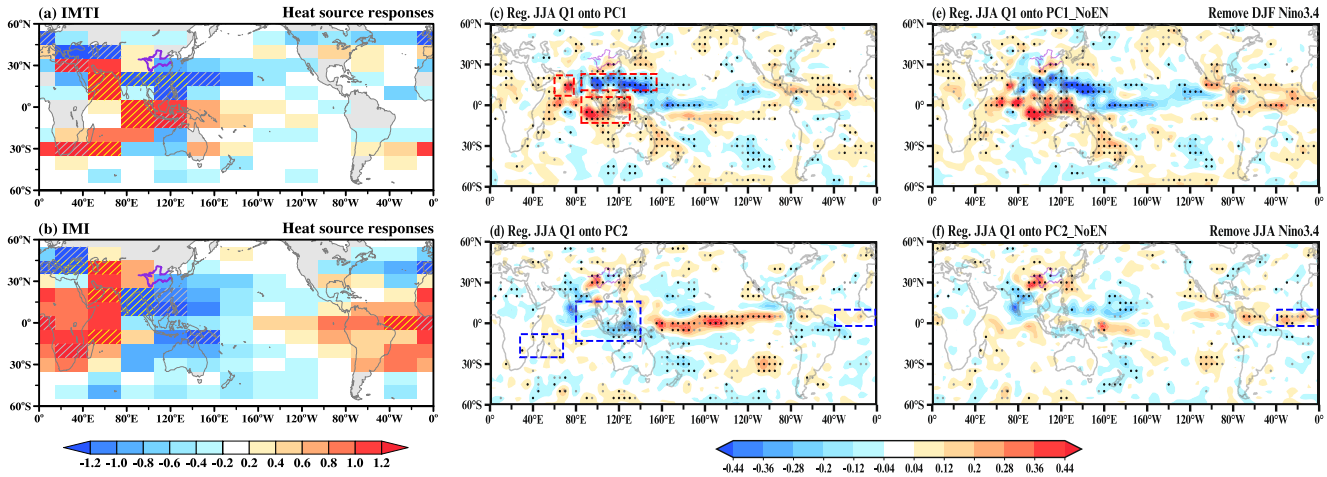

Figure 2. The normalized (a) IMTI and (b) IMI for each of the 132-member simulations in the LBM Green's function experiment in terms of the geographic location of the heat sources. Values exceeding the 90th (95th) percentile thresholds are hatched in gray (yellow), calculated by sorting the absolute values in ascending order. The Q_1 (shading; K day^{-1}) in JJA regressed onto the (c) PC1, (d) PC2, (e) PC1_NoEN, and (f) PC2_NoEN, respectively. Gray (black) dots indicate regression coefficients passing the 90% (95%) confidence level. The red dashed boxes in (c) denote regions of the Arabian Sea (7°–22°N, 60°–78°E), tropical EIO-MC (13°S–6°N, 85°–130°E), and BOB-WNP (11°–23°N, 85°–155°E), respectively. The blue dashed boxes in (d) denote regions of the tropical SWIO (8°–25°S, 28°–68°E), equatorial Atlantic (2°S–10°N, 0°–39°W), and tropical EIO-WP (13°S–16°N, 80°–140°E), respectively.

observations, the linear regression analysis cannot identify the casual relationship between SASM and diabatic heating anomalies, whereas the LBM can capture the independent impact of heat sources.

The experimental results show the sensitivity of the first two SASM modes to certain heat sources, while observations indicate their likelihood of occurrence. The heat source that both significantly triggers SASM modes in experiments and likely occurs in observations can effectively influence SASM. Therefore, we define an optimal heat source pattern for the SASM modes based on two criteria: (a) experimental heat sources that simulate IMTI or IMI values above the 90th percentile thresholds, and (b) observed heat sources (Q_1) regressed onto PC1 or PC2 passing the 90% confidence level. Considering both, the optimal atmospheric heat sources for the first SASM mode include diabatic heating over the Arabian Sea and tropical EIO-MC, and cooling over the BOB-WNP. For the second mode, diabatic heating over the tropical SWIO and equatorial Atlantic, and cooling over the tropical EIO-WP are identified. In observations, potential heat source interactions influence the significance in some regions, so we used the 90% confidence level to identify optimal patterns. Since signals are more prominent in the tropics, we focus on the tropical heat sources here. Note that extratropical heat sources may also contribute to SASM anomalies. In the LBM Green's function experiment, the second SASM mode is also associated with heating anomalies in the subtropical regions such as the West Asia, consistent with previous studies (Ding & Wang, 2005; Zhang et al., 2022).

Notably, the observed heat source over equatorial Atlantic is not as significant as that in the experiment due to the complex impact of multi-ocean interactions. To verify the importance of the observed equatorial Atlantic heat source, Figure 2f shows Q_1 related to the PC2_NoEN (linearly removing the JJA Niño3.4 from PC2), revealing significant diabatic heating over equatorial Atlantic. This indicates that ENSO-induced heat sources can partially cover the significant impact of the equatorial Atlantic heat source, which can be captured by the experiment since the heat sources are independent of one another in LBM. Indeed, equatorial Atlantic SSTAs can influence South Asia by stimulating eastward-propagating Kelvin waves through local heat sources (Jiang & Li, 2021; Kucharski et al., 2007, 2008; Sabeerali et al., 2019), contributing to the establishment of an anomalous anticyclone over central-northern India. LBM experiment also shows that the equatorial Atlantic heat source can cause anomalous easterlies over tropical North Indian Ocean and lead to anticyclonic shear over South Asia (Figure S3e in Supporting Information S1).

To further confirm the role of optimal atmospheric heat sources, we used the LBM to investigate the responses of lower-level circulation to the combinations of optimal heat sources above. Diabatic heating/cooling with a peak of 2 K day^{-1} at the 0.45 sigma level was imposed at locations corresponding to the optimal heat sources. For the first SASM mode, the combination of three diabatic forcings can well reproduce the lower-level anomalous

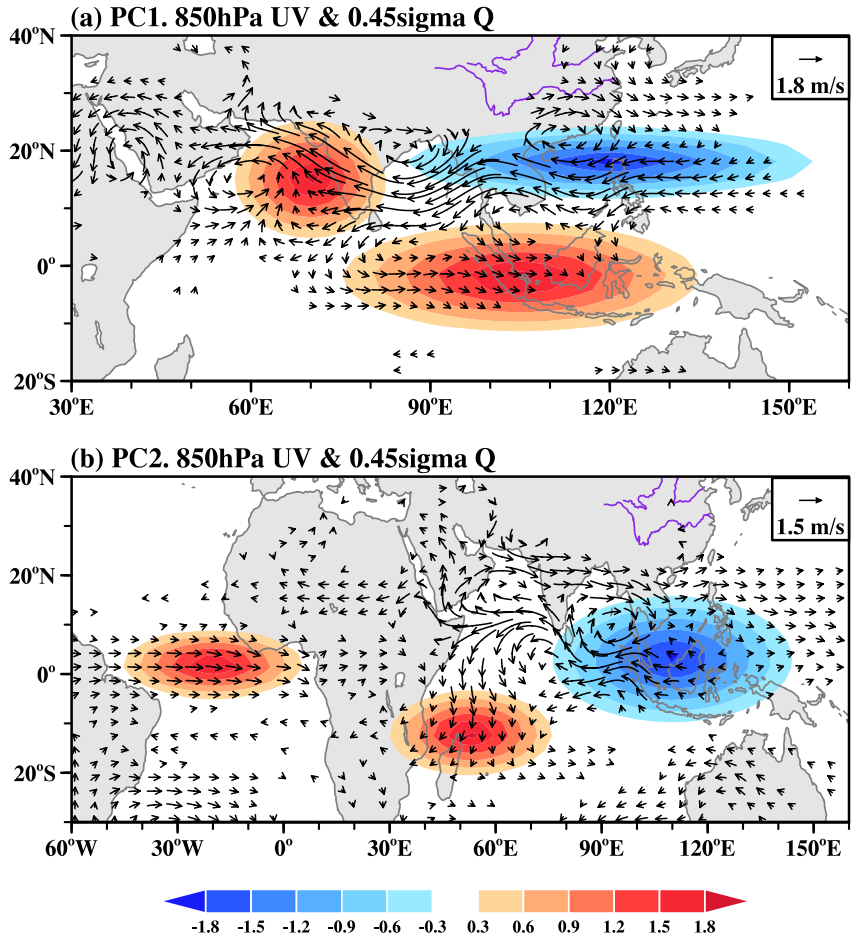

Figure 3. Steady responses of 850-hPa winds to the diabatic forcings for (a) PC1 with the combination of heating over the Arabian Sea, tropical EIO-MC, and cooling over the BOB-WNP. (b) As in (a), but for PC2 with the combination of heating over the tropical SWIO, equatorial Atlantic, and cooling over the tropical EIO-WP.

anticyclones over the northern BOB and WNP with pronounced easterlies around 15°N (Figure 3a). For the second SASM mode, the anomalous anticyclone over central-northern India and easterlies over the northern Arabian Sea are stimulated by the diabatic forcings (Figure 3b). The consistent results of observations and models suggest the identified optimal heat sources are reasonable and effective. Figure S3 in Supporting Information S1 illustrates the independent roles of each heat source. Although the heat source over SWIO may be influenced to some extent by ENSO (Figure 2f), it can still exert an independent effect on the second SASM mode through the cross-equatorial circulation.

3.3. Optimal Atmospheric Heat Sources as a Bridge in the ENSO–SASM Relationship

Indices of optimal heat sources (I_{Q_1}) over the Arabian Sea, tropical EIO-MC, and BOB-WNP for PC1; and over tropical SWIO, equatorial Atlantic, and tropical EIO-WP for PC2 were calculated by the local averaged Q_1 weighted by regression coefficients with respect to PC1 and PC2, respectively (T. Lu et al., 2023):

$$I_{Q_1} = \frac{Q_{11}b_1 + Q_{12}b_2 + \ldots + Q_{1n}b_n}{b_1 + b_2 + \ldots + b_n}, \quad (2)$$

Here, the n denotes the number of significant grids, b_k ($k = 1, 2, \ldots, n$) represents the k th regression coefficient (passing the 90% confidence level), and Q_{1k} refers to the corresponding Q_1.

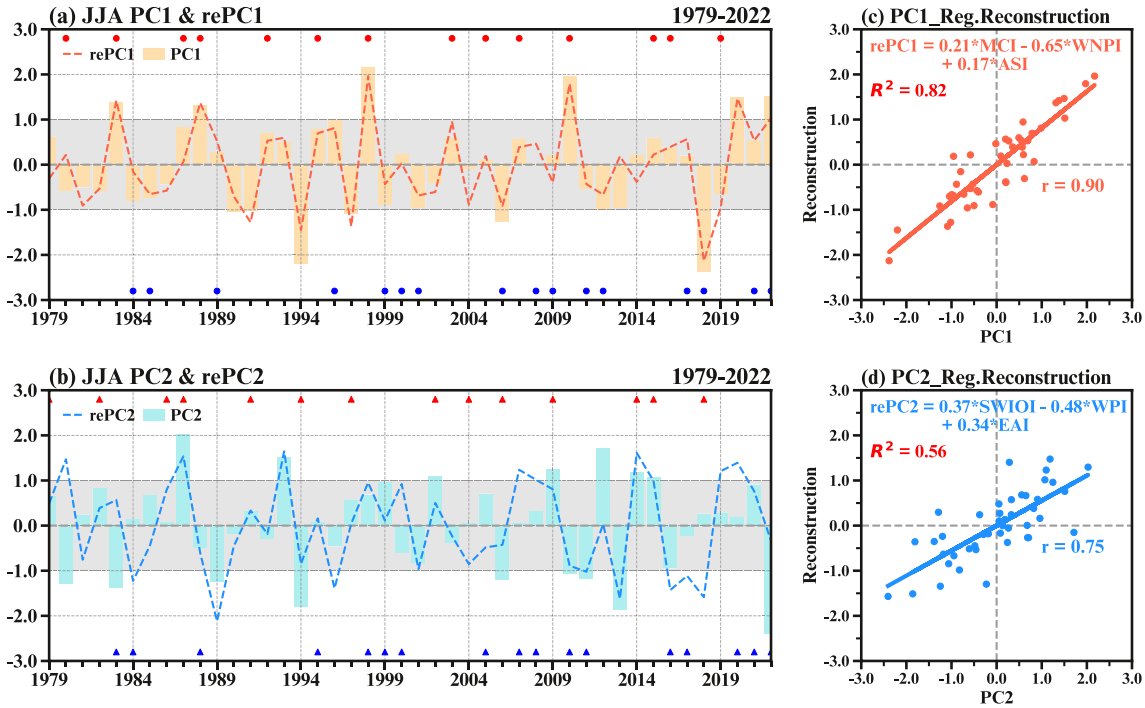

Figure 4. (a) The standardized PC1 (orange bars) and rePC1 (orange dashed lines) in JJA. (b) As in (a), but for PC2 (blue bars) and rePC2 (blue dashed lines). Values above and below the gray zone (one standard deviation interval) represent the abnormally positive and negative years, respectively. The red/blue dots (triangles) have the same meaning as in Figures 1c and 1d. (c and d) Scatterplots for (c) PC1 and (d) PC2 with respect to rePC1 and rePC2, respectively. The equations are multiple linear regression models, with the independent variables being JJA I_{Q_1} over the Arabian Sea (ASI), tropical EIO-MC (MCI), and BOB-WNP (WNPI) for PC1, and over the tropical SWIO (SWIOI), equatorial Atlantic (EAI), and tropical EIO-WP (WPI) for PC2.

To evaluate the overall explanatory power of I_{Q_1} for the two leading SASM modes, we established multiple linear regression models for PC1 and PC2, with JJA I_{Q_1} as the independent variables (Figures 4c and 4d), passing the *F*-test (Slinker & Glantz, 1988). These indices explain 82% of the variance in PC1 ($R^2 = 0.82$) with a correlation of 0.90 between the reconstructed PC1 (rePC1) and PC1. Similarly, the I_{Q_1} indices explain 56% of the variance in PC2 with a correlation of 0.75 between rePC2 and PC2. These findings underscore the significant contributions of optimal heat sources to the two leading SASM modes.

The variability of PCs and rePCs shows a strong consistency, especially during abnormal years (Figures 4a and 4b), corresponding to ENSO events, the dominant climate mode influencing SASM (Pant & Parthasarathy, 1981; Webster & Yang, 1992). Diabatic heating regressed onto DJF Niño3.4 aligns with the optimal pattern for PC1 (Figure S4a in Supporting Information S1). Even after linearly removing DJF Niño3.4, heat sources related to PC1_NoEN remains similar to the optimal pattern (Figure 2e), indicating it is directly driven by tropical Indian Ocean SSTAs. These SSTAs store ENSO effects during winter and activate via the IPOC mode in the following summer, explaining the strong correlation between ENSO decaying phase and the first SASM mode (Chowdary et al., 2019; Xie et al., 2009). Similarly, the significant correlation between ENSO developing phase and the second SASM mode is driven by tropical eastern Pacific SSTAs, anchoring descending branch of the anomalous Walker circulation to the tropical EIO-WP, inducing local diabatic cooling important for PC2 (Figure S4b in Supporting Information S1; P. Hu et al., 2024; B. Wang et al., 2017).

However, during some ENSO years, the diabatic heating patterns are inconsistent with or offset the optimal patterns. For example, in 1989 (La Niña decaying year), the JJA heating pattern is inconsistent with the optimal pattern for PC1. In 1986 (El Niño developing year), only the SWIO heat source aligns with the optimal pattern for PC2, while those over tropical EIO-WP and equatorial Atlantic oppose it, leading to their impacts offsetting each other (Figures S5a and S5b in Supporting Information S1). Such misalignments weaken ENSO's influence on SASM, indicating an unstable ENSO–SASM relationship. As shown in Figures 2e and 2f, ENSO-related heat sources are part of the optimal patterns. Other SSTA modes, like those over equatorial Atlantic, can also

independently generate similar heat sources. For instance, in 2013 (non-ENSO year), the heat sources oppose PC2's optimal pattern, leading to a negative SASM anomaly. Similarly, in 2020, it aligns with the optimal pattern of PC1, causing a positive anomaly (Figures S5c and S5d in Supporting Information S1).

4. Summary

This study identified the optimal atmospheric heat sources for the dominant modes of SASM interannual variability based on the LBM Green's function experiment. For the first SASM mode, characterized by a lower-level anomalous anticyclone over the northern BOB and a remarkable tripolar terrestrial precipitation pattern, the optimal atmospheric heating is distributed over the Arabian Sea and tropical EIO-MC, with cooling over the BOB-WNP. In contrast, heating over the tropical SWIO and equatorial Atlantic, along with cooling over the tropical EIO-WP, optimally drives the second SASM mode, which features a lower-level anomalous anticyclone and negative precipitation anomalies over central-northern India.

ENSO can indirectly influence SASM interannual variability. During ENSO decaying phase, heat sources triggered by the IPOC mode resemble the optimal pattern of PC1, while during ENSO developing phase, heat sources over the tropical EIO-WP induced by the anomalous Walker circulation match the optimal pattern of PC2. The alignment between ENSO-related heat sources and optimal patterns leads to the significant ENSO–SASM relationship. When heat sources induced by ENSO are inconsistent with or offset the optimal patterns, ENSO's impact on SASM weakens, resulting in an unstable ENSO–SASM relationship (Chang et al., 2001; Kumar et al., 1999). In addition to ENSO, other SSTA modes, such as the Atlantic Zonal Mode (Sabeerali et al., 2019), can also generate similar heating patterns independently, causing corresponding SASM anomalies. It can be captured by the experiment because the heat sources are independent of one another in LBM.

The concept of optimal atmospheric heat sources provides a new perspective for understanding the ENSO–SASM relationship and may help improve the SASM prediction under complex multi-ocean interactions. Further research is needed to investigate the preceding SST signals that contribute to the formation of these optimal heat sources. Additionally, the influence of nonlinear interactions between different heat sources on the accuracy of this linear method's results also merits further investigation.

Data Availability Statement

The HadISST data set (Rayner et al., 2003) is available at https://www.metoffice.gov.uk/hadobs/hadisst/. The CRU TS v.4.07 data set (Harris et al., 2020) is openly obtained at https://crudata.uea.ac.uk/cru/data/hrg/. The ERA5 data set can be obtained from Hersbach et al. (2023). The NCEP2 data set (Kanamitsu et al., 2002) can be downloaded from https://psl.noaa.gov/data/gridded/data.ncep.reanalysis2.html. The data from the LBM simulations have been made publicly available via a data repository at T. Lu (2024).

Acknowledgments
This work is supported by the National Natural Science Foundation of China (Grants 42175040, 42141019, 42261144687, 42475046) and the Youth Innovation Promotion Association of CAS (2021072). Tong Lu thanks Suqin Zhang, Peng Hu, and Haosu Tang for helpful discussions and advice.

References

Ashok, K., Guan, Z., & Yamagata, T. (2001). Impact of the Indian Ocean dipole on the relationship between the Indian monsoon rainfall and ENSO. *Geophysical Research Letters*, *28*(23), 4499–4502. https://doi.org/10.1029/2001GL013294

Bloch-Johnson, J., Rugenstein, M. A. A., Alessi, M. J., Proistosescu, C., Zhao, M., Zhang, B., et al. (2024). The Green's function model intercomparison project (GFMIP) protocol. *Journal of Advances in Modeling Earth Systems*, *16*(2), e2023MS003700. https://doi.org/10.1029/2023MS003700

Branstator, G. (1985). Analysis of general circulation model sea-surface temperature anomaly simulations using a linear model. Part I: Forced solutions. *Journal of the Atmospheric Sciences*, *42*(21), 2225–2241. https://doi.org/10.1175/1520-0469(1985)042<2225:AOGCMS>2.0.CO;2

Chang, C., Harr, P., & Ju, J. (2001). Possible roles of Atlantic circulations on the weakening Indian monsoon rainfall–ENSO relationship. *Journal of Climate*, *14*(11), 2376–2380. https://doi.org/10.1175/1520-0442(2001)014<2376:PROACO>2.0.CO;2

Chowdary, J. S., Patekar, D., Srinivas, G., Gnanaseelan, C., & Parekh, A. (2019). Impact of the Indo-Western Pacific Ocean capacitor mode on South Asian summer monsoon rainfall. *Climate Dynamics*, *53*(3–4), 2327–2338. https://doi.org/10.1007/s00382-019-04850-w

Darshana, P., Chowdary, J. S., Parekh, A., & Gnanaseelan, C. (2022). Relationship between the Indo-Western Pacific Ocean capacitor mode and Indian summer monsoon rainfall in CMIP6 models. *Climate Dynamics*, *59*(1), 393–415. https://doi.org/10.1007/s00382-021-06133-9

Ding, Q., & Wang, B. (2005). Circumglobal teleconnection in the Northern Hemisphere summer. *Journal of Climate*, *18*(17), 3483–3505. https://doi.org/10.1175/JCLI3473.1

Emanuel, K. A., Neelin, J. D., & Bretherton, C. S. (1994). On large-scale circulations in convecting atmospheres. *Quarterly Journal of the Royal Meteorological Society*, *120*(519), 1111–1143. https://doi.org/10.1002/qj.49712051902

Gill, A. E. (1980). Some simple solutions for heat-induced tropical circulation. *Quarterly Journal of the Royal Meteorological Society*, *106*(449), 447–462. https://doi.org/10.1002/qj.49710644905

Harris, I., Osborn, T. J., Jones, P., & Lister, D. (2020). Version 4 of the CRU TS monthly high-resolution gridded multivariate climate dataset [Dataset]. *Scientific Data*, *7*(1), 109. https://doi.org/10.1038/s41597-020-0453-3

Harrop, B. E., Lu, J., Liu, F., Garuba, O. A., & Leung, L. R. (2018). Sensitivity of the ITCZ location to ocean forcing via q-flux Green's function experiments. *Geophysical Research Letters*, *45*(23), 13116–13123. https://doi.org/10.1029/2018GL080772

Hersbach, H., Bell, B., Berrisford, P., Biavati, G., Horányi, A., Muñoz Sabater, J., et al. (2023). ERA5 monthly averaged data on pressure levels from 1940 to present [Dataset]. *Copernicus Climate Change Service (C3S) Climate Data Store (CDS)*. https://doi.org/10.24381/cds.6860a573

Hoskins, B. J., & Rodwell, M. J. (1995). A model of the Asian summer monsoon. Part I: The global scale. *Journal of the Atmospheric Sciences*, *52*(9), 1329–1340. https://doi.org/10.1175/1520-0469(1995)052<1329:AMOTAS>2.0.CO;2

Hu, K., & Long, S.-M. (2019). Optimal heat source for the interannual variability of the western North Pacific summer monsoon. *Atmospheric and Oceanic Science Letters*, *13*(1), 41–47. https://doi.org/10.1080/16742834.2019.1680087

Hu, P., Chen, W., Chen, S., Liu, Y., Wang, L., & Huang, R. (2022). The leading mode and factors for coherent variations among the subsystems of tropical Asian summer monsoon onset. *Journal of Climate*, *35*(5), 1597–1612. https://doi.org/10.1175/JCLI-D-21-0101.1

Hu, P., Chen, W., Chen, S., Yang, R., Wang, L., & Liu, Y. (2024). Revisiting the linkage between the Pacific–Japan pattern and Indian summer monsoon rainfall: The crucial role of the Maritime Continent. *Geophysical Research Letters*, *51*(3), e2023GL106982. https://doi.org/10.1029/2023GL106982

Jiang, L., & Li, T. (2021). Impacts of tropical North Atlantic and equatorial Atlantic SST anomalies on ENSO. *Journal of Climate*, *34*(14), 5635–5655. https://doi.org/10.1175/JCLI-D-20-0835.1

Kanamitsu, M., Ebisuzaki, W., Woollen, J., Yang, S.-K., Hnilo, J., Fiorino, M., & Potter, G. (2002). NCEP–DOE AMIP-II reanalysis (R-2) [Dataset]. *Bulletin of the American Meteorological Society*, *83*(11), 1631–1644. https://doi.org/10.1175/BAMS-83-11-1631

Kucharski, F., Bracco, A., Yoo, J. H., & Molteni, F. (2007). Low-frequency variability of the Indian monsoon–ENSO relationship and the tropical Atlantic: The "weakening" of the 1980s and 1990s. *Journal of Climate*, *20*(16), 4255–4266. https://doi.org/10.1175/JCLI4254.1

Kucharski, F., Bracco, A., Yoo, J. H., & Molteni, F. (2008). Atlantic forced component of the Indian monsoon interannual variability. *Geophysical Research Letters*, *35*(4), L04706. https://doi.org/10.1029/2007GL033037

Kumar, K. K., Rajagopalan, B., & Cane, M. A. (1999). On the weakening relationship between the Indian monsoon and ENSO. *Science*, *284*(5423), 2156–2159. https://doi.org/10.1126/science.284.5423.2156

Kumar, K. K., Rajagopalan, B., Hoerling, M., Bates, G., & Cane, M. (2006). Unraveling the mystery of Indian monsoon failure during El Niño. *Science*, *314*(5796), 115–119. https://doi.org/10.1126/science.1131152

Li, B., Zhou, L., Qin, J., Zhou, T., Chen, D., Hou, S., & Murtugudde, R. (2023). Middle east warming in spring enhances summer rainfall over Pakistan. *Nature Communications*, *14*(1), 7635. https://doi.org/10.1038/s41467-023-43463-0

Lin, S., Dong, B., Yang, S., & Zhang, T. (2024). Diverse impacts of the Indian summer monsoon on ENSO among CMIP6 models and its possible causes. *Environmental Research Letters*, *19*(8), 084052. https://doi.org/10.1088/1748-9326/ad6618

Lin, S., Yang, S., He, S., Fan, H., Chen, J., Dong, W., et al. (2023). Atmospheric–oceanic processes over the Pacific involved in the effects of the Indian summer monsoon on ENSO. *Journal of Climate*, *36*(17), 6021–6043. https://doi.org/10.1175/JCLI-D-22-0822.1

Liu, F., Lu, J., Garuba, O., Leung, L. R., Luo, Y., & Wan, X. (2018). Sensitivity of surface temperature to oceanic forcing via q-flux Green's function experiments. Part I: Linear response function. *Journal of Climate*, *31*(9), 3625–3641. https://doi.org/10.1175/JCLI-D-17-0462.1

Liu, F., Lu, J., & Leung, L. R. (2022). Neutral mode dominates the forced global and regional surface temperature response in the past and future. *Geophysical Research Letters*, *49*(15), e2022GL098788. https://doi.org/10.1029/2022GL098788

Lu, J., Liu, F., Leung, L. R., & Lei, H. (2020). Neutral modes of surface temperature and the optimal ocean thermal forcing for global cooling. *Npj Climate and Atmospheric Science*, *3*(1), 9. https://doi.org/10.1038/s41612-020-0112-6

Lu, R., & Lin, Z. (2009). Role of subtropical precipitation anomalies in maintaining the summertime meridional teleconnection over the western North Pacific and East Asia. *Journal of Climate*, *22*(8), 2058–2072. https://doi.org/10.1175/2008JCLI2444.1

Lu, T. (2024). Data of LBM simulations [Dataset]. https://doi.org/10.5281/zenodo.13324534

Lu, T., Zhu, Z., Yang, Y., Ma, J., & Huang, G. (2023). Formation mechanism of the ENSO-independent summer western North Pacific anomalous anticyclone. *Journal of Climate*, *36*(6), 1711–1726. https://doi.org/10.1175/JCLI-D-22-0271.1

Mishra, V., Smoliak, B. V., Lettenmaier, D. P., & Wallace, J. M. (2012). A prominent pattern of year-to-year variability in Indian summer monsoon rainfall. *Proceedings of the National Academy of Sciences of the United States of America*, *109*(19), 7213–7217. https://doi.org/10.1073/pnas.1119150109

North, G. R., Bell, T. L., Cahalan, R. F., & Moeng, F. J. (1982). Sampling errors in the estimation of empirical orthogonal functions. *Monthly Weather Review*, *110*(7), 699–706. https://doi.org/10.1175/1520-0493(1982)110<0699:SEITEO>2.0.CO;2

Pant, G., & Parthasarathy, S. B. (1981). Some aspects of an association between the southern oscillation and Indian summer monsoon. *Archives for Meteorology, Geophysics, and Bioclimatology Series B*, *29*(3), 245–252. https://doi.org/10.1007/bf02263246

Rajeevan, M., & Sridhar, L. (2008). Inter-annual relationship between Atlantic sea surface temperature anomalies and Indian summer monsoon. *Geophysical Research Letters*, *35*(21), L21704. https://doi.org/10.1029/2008GL036025

Rayner, N., Parker, D. E., Horton, E., Folland, C. K., Alexander, L. V., Rowell, D., et al. (2003). Global analyses of sea surface temperature, sea ice, and night marine air temperature since the late nineteenth century [Dataset]. *Journal of Geophysical Research*, *108*(D14), 4407. https://doi.org/10.1029/2002JD002670

Sabeerali, C. T., Ajayamohan, R. S., Bangalath, H. K., & Chen, N. (2019). Atlantic zonal mode: An emerging source of Indian summer monsoon variability in a warming world. *Geophysical Research Letters*, *46*(8), 4460–4467. https://doi.org/10.1029/2019GL082379

Slinker, B. K., & Glantz, S. A. (1988). Multiple linear regression is a useful alternative to traditional analyses of variance. *American Journal of Physiology - Regulatory, Integrative and Comparative Physiology*, *255*(3), R353–R367. https://doi.org/10.1152/ajpregu.1988.255.3.R353

Song, Q., Wang, C., Yao, Y., & Fan, H. (2024). Unraveling the Indian monsoon's role in fueling the unprecedented 2022 marine heatwave in the western North Pacific. *Npj Climate and Atmospheric Science*, *7*(1), 90. https://doi.org/10.1038/s41612-024-00645-x

Tang, H., Wang, J., Hu, K., Huang, G., Chowdary, J. S., Wang, Y., et al. (2022). Increasing 2020-like boreal summer rainfall extremes over Northeast Indian subcontinent under greenhouse warming. *Geophysical Research Letters*, *49*(11), e2021GL096377. https://doi.org/10.1029/2021GL096377

Tang, S., Qiao, S., Wang, B., Liu, F., Feng, T., Yang, J., et al. (2023). Linkages of unprecedented 2022 Yangtze River Valley heatwaves to Pakistan flood and triple-dip La Niña. *Npj Climate and Atmospheric Science*, *6*(1), 44. https://doi.org/10.1038/s41612-023-00386-3

Turner, A. G., & Annamalai, H. (2012). Climate change and the South Asian summer monsoon. *Nature Climate Change*, *2*(8), 587–595. https://doi.org/10.1038/nclimate1495

Wang, B. (1992). The vertical structure and development of the ENSO anomaly mode during 1979–1989. *Journal of the Atmospheric Sciences*, *49*(8), 698–712. https://doi.org/10.1175/1520-0469(1992)049<0698:TVSADO>2.0.CO;2

Wang, B., Li, J., & He, Q. (2017). Variable and robust East Asian monsoon rainfall response to El Niño over the past 60 years (1957–2016). *Advances in Atmospheric Sciences*, *34*(10), 1235–1248. https://doi.org/10.1007/s00376-017-7016-3

Wang, B., Wu, R., & Lau, K. (2001). Interannual variability of the Asian summer monsoon: Contrasts between the Indian and the western North Pacific–East Asian monsoons. *Journal of Climate*, *14*(20), 4073–4090. https://doi.org/10.1175/1520-0442(2001)014<4073:IVOTAS>2.0.CO;2

Wang, Y., Hu, K., Huang, G., & Tao, W. (2023). The role of nonlinear energy advection in forming asymmetric structure of ENSO teleconnections over the North Pacific and North America. *Geophysical Research Letters*, *50*(17), e2023GL105277. https://doi.org/10.1029/2023GL105277

Watanabe, M., & Kimoto, M. (2000). Atmosphere-ocean thermal coupling in the North Atlantic: A positive feedback. *Quarterly Journal of the Royal Meteorological Society*, *126*(570), 3343–3369. https://doi.org/10.1002/qj.49712657017

Webster, P. J., & Yang, S. (1992). Monsoon and ENSO: Selectively interactive systems. *Quarterly Journal of the Royal Meteorological Society*, *118*(507), 877–926. https://doi.org/10.1002/qj.49711850705

Wu, R. (2017). Relationship between Indian and East Asian summer rainfall variations. *Advances in Atmospheric Sciences*, *34*(1), 4–15. https://doi.org/10.1007/s00376-016-6216-6

Wu, Y., Lu, J., Ding, Q., & Liu, F. (2021). Linear response function reveals the most effective remote forcing in causing September Arctic Sea ice melting in CESM. *Geophysical Research Letters*, *48*(15), e2021GL094189. https://doi.org/10.1029/2021GL094189

Xiang, B., & Wang, B. (2013). Mechanisms for the advanced Asian summer monsoon onset since the mid-to-Late 1990s. *Journal of Climate*, *26*(6), 1993–2009. https://doi.org/10.1175/JCLI-D-12-00445.1

Xie, S.-P., Hu, K., Hafner, J., Tokinaga, H., Du, Y., Huang, G., & Sampe, T. (2009). Indian Ocean capacitor effect on Indo–Western Pacific climate during the summer following El Niño. *Journal of Climate*, *22*(3), 730–747. https://doi.org/10.1175/2008JCLI2544.1

Xie, S.-P., Kosaka, Y., Du, Y., Hu, K., Chowdary, J. S., & Huang, G. (2016). Indo-Western Pacific Ocean capacitor and coherent climate anomalies in post-ENSO summer: A review. *Advances in Atmospheric Sciences*, *33*(4), 411–432. https://doi.org/10.1007/s00376-015-5192-6

Yanai, M., Esbensen, S., & Chu, J.-H. (1973). Determination of bulk properties of tropical cloud clusters from large-scale heat and moisture budgets. *Journal of the Atmospheric Sciences*, *30*(4), 611–627. https://doi.org/10.1175/1520-0469(1973)030<0611:DOBPOT>2.0.CO;2

Yu, S. Y., Fan, L., Zhang, Y., Zheng, X. T., & Li, Z. (2021). Reexamining the Indian summer monsoon rainfall–ENSO relationship from its recovery in the 21st century: Role of the Indian Ocean SST anomaly associated with types of ENSO evolution. *Geophysical Research Letters*, *48*(12), e2021GL092873. https://doi.org/10.1029/2021GL092873

Zhang, T., Jiang, X., Yang, S., Chen, J., & Li, Z. (2022). A predictable prospect of the South Asian summer monsoon. *Nature Communications*, *13*(1), 7080. https://doi.org/10.1038/s41467-022-34881-7

Zhou, Z. Q., Xie, S. P., & Zhang, R. (2019). Variability and predictability of Indian rainfall during the monsoon onset month of June. *Geophysical Research Letters*, *46*(24), 14782–14788. https://doi.org/10.1029/2019GL085495